

# Resonance Raman spectroscopy in the dissociative A band of nitrosyl chloride

Jeffrey L. Mackey,<sup>a)</sup> Bruce R. Johnson, Carter Kittrell, Linh D. Le,<sup>b)</sup> and James L. Kinsey  
*Department of Chemistry and Rice Quantum Institute, Rice University, MS 600, Houston,  
Texas 77251-1892*

(Received 30 November 2000; accepted 24 January 2001)

Resonance Raman spectra measured for ClNO photoexcited at 212.5, 219, and 222 nm produce evidence that the strong transition at the vacuum ultraviolet end of the merged A band system dominates to wavelengths as long as 222 nm. The spectral resolution is sufficient to enable definitive assignments of excited vibrational levels in the ground electronic state, several of which have not been previously observed. A curvilinear coordinate model of the ground state potential surface around the Franck–Condon region has been constructed. This model yields vibrational eigenvalues in excellent agreement with all known transitions. © 2001 American Institute of Physics.

[DOI: 10.1063/1.1355656]

## I. INTRODUCTION

Ultraviolet photoexcitation of nitrosyl chloride (ClNO) in the A band ( $\lambda \sim 180\text{--}250\text{ nm}$ ) produces Cl and NO photofragments.<sup>1</sup> (The band was named before current naming conventions were established, and so the A band lies above the B, C, etc., bands in energy.) The A band is intense, with an absorption cross section of approximately  $6.5 \times 10^{-17}\text{ cm}^2$  at its peak near 196 nm wavelength.<sup>2,3</sup> The breadth of the band [ $\sim 5000\text{ cm}^{-1}$  full width at half maximum (FWHM)] and absence of structure indicate rapid and direct dissociation following excitation. It has been suggested that as many as three electronically excited states may participate in the absorption,<sup>4–6</sup> with the proportion from each state varying with wavelength within the band. This supposition is not unequivocally established, however, and runs counter to the prediction of *ab initio* calculations on ClNO.<sup>7,8</sup>

Despite a large number of studies of the photofragments,<sup>4–6,9–12</sup> a complete picture of the photodissociation is still elusive. Raman spectroscopy, while it cannot resolve all the mysteries, can in certain cases identify overlapped transitions through interference in fundamental transition intensities viewed as functions of excitation wavelength.<sup>13,14</sup> In addition, when the excitation is into a dissociative continuum, Raman spectra produce long progressions of vibrational modes in the ground electronic state, thereby yielding information about the ground state potential energy surface (PES). At the same time, Raman spectroscopy carried out with sufficient care is able to provide unique insight into the early femtoseconds of direct dissociation in the excited state.<sup>15–17</sup>

While such results have now been obtained for a variety of directly dissociating molecules,<sup>18</sup> the only ClNO Raman

results published to date come from a low resolution study at an excitation wavelength of 266 nm by Bell and Frey.<sup>19</sup> At this far red edge of the A band the absorption cross section has dropped to  $1.4 \times 10^{-19}\text{ cm}^2$ ,  $\sim 0.2\%$  the value at band peak. These experiments revealed a sequence of about 12 vibrational features out to a Raman shift of  $\sim 3400\text{ cm}^{-1}$ , the isolated  $\nu_3$  peak at  $332\text{ cm}^{-1}$  being the most intense. The  $\nu_1$  fundamental ( $1800\text{ cm}^{-1}$ ) was completely absent. Their instrumental resolution was insufficient to cleanly resolve the  $\nu_2$  ( $\sim 596\text{ cm}^{-1}$ ) and  $2\nu_3$  ( $662\text{ cm}^{-1}$ ) bands, and there were similar merged features at higher Raman shifts. No detailed analysis was possible at the time.

Our work examines Raman emission spectra of ClNO using significantly higher resolution and shorter wavelengths (i.e., toward the center of the A band). At 212.5, 219, and 222 nm, the absorption cross sections are, respectively, about  $2.1 \times 10^{-17}$ ,  $1.0 \times 10^{-17}$ , and  $0.7 \times 10^{-17}\text{ cm}^2$ .<sup>3</sup> There is no striking evidence of electronic interference at these wavelengths, suggesting that a single electronic state is important in the direct absorption in this wavelength range. This result is placed in the context of recent assignments in a discussion below.

The primary result of the current paper is the development of a model capable of accurately reproducing all of the vibrational levels that have been observed. Of these, a significant fraction are reported for the first time. The large-amplitude vibrational model is fully curvilinear, with numerically converged three-dimensional (3D) eigenvalues all giving transitions within a few  $\text{cm}^{-1}$  of the experimental values. A unique aspect of this model construction turns out to be the appropriateness of curvilinear Jacobi coordinates for the vibrational motion in the vicinity of the ground electronic state equilibrium geometry. This model will serve as the basis for a subsequent treatment of the dissociation dynamics using solution of the time-dependent Schrödinger equation in a wavelet basis.

In Sec. II of this paper, the experimental apparatus is described. Section III contains the experimental results and

<sup>a)</sup>Permanent address: Micron Technology, Inc., MS 306, 8000 Federal Way, Boise, Idaho 83707-0006.

<sup>b)</sup>Permanent address: The Dow Chemical Company, Bldg. 2504, P.O. Box 400, Plaquemine, Louisiana 70765.

compares the Raman spectra at three different excitation wavelengths. The significance of the results with respect to recent interpretations of the *A* band is discussed. Section IV presents the vibrational analysis, including both a Dunham expansion and a potential expansion in Jacobi coordinates believed to be accurate in the Franck–Condon region and somewhat beyond. Section V gives the conclusions.

## II. EXPERIMENT

Light generation for these experiments begins with a Questek 2670 XeCl excimer laser operating at 308 nm, with 10 ns pulses of 100–300 mJ energy. Shot-to-shot fluctuations in the total output energy for a given set of operating parameters are on the order of  $\pm 20\%$ . The rectangular ( $2.5 \times 1.3$  cm) excimer beam enters a Lambda Physik FL 3002 dye laser, which converts the light to visible wavelengths with a roughly circular profile ( $\sim 1.5$  mm) and energies on the order of 2 mJ per pulse. Coumarin 440 and Stilbene 420 dyes were used in this work. The visible light from the dye laser passes through a beta-barium borate ( $\beta$ -BBO) frequency-doubling crystal to produce ultraviolet (UV) wavelengths down to about 207 nm. Unconverted visible light and UV light are separated by passing the mixed beam through a self-compensating set of four-prisms, and blocking the visible light. Typical pulse energies after conversion and separation range from 5–60  $\mu$ J/pulse. The UV light is steered into a scattering cell where it intersects the sample flow at  $90^\circ$ .

A flowing gas system is used to prevent sample depletion by the UV pulses and to avoid the buildup of significant concentrations of photoproducts that may provide spectral interference. The gas flow system is designed to bring the gas phase sample into the target region of the flow cell in a highly reproducible and controllable manner. Carrier gas (He) flows into a wide-diameter ( $\sim 2.5$  cm) fritted bubbler immersed in liquid CINO held at approximately  $-58^\circ\text{C}$  by a refrigerated ethanol bath. This provides a stable concentration of CINO mixed with the carrier gas and carried into the cell through a vertical  $1/4''$  stainless steel tube. A roughly cylindrical shell of carrier gas surrounds the flowing sample to keep it collimated and localized at the center of the cell. The flow rate of the coaxial shell is roughly twice that of the sample gas, optimal conditions being determined beforehand from examination of the white smoke produced by passage of pre-mixed  $\text{NH}_3/\text{HCl}$  with helium as a carrier gas. Window purges of pure He protect the front and rear cell windows and an internal light collection lens.

All gases exit through an aperture at the bottom of the cell for release into a fume hood. During data acquisition, the total pressure in the cell remains at approximately one atmosphere.

The data acquisition system includes the light collection optics, a grating monochromator, a photomultiplier detector, and computer hardware/software for storing the data and running the experiment. The Czerny–Turner monochromator (Spex model 1402) has a focal length of 0.75 m. A Spectronic Instruments 100 mm square holographic diffraction grating with 2400 sinusoidal grooves per mm was used. The optical axis of the monochromator provides a fixed spatial

direction in the system. The gas flow and the incident laser light are both capable of being positioned to match this axis.

The light passing through the monochromator impinges onto a solar blind photomultiplier tube (PMT), Hamamatsu model number R166HA, operated at  $\sim 750$  volts to  $\sim 1200$  volts depending on signal strength. The output of the PMT passes through a SRS-250 gated integrator, then through a coax cable delay line to allow the prior arrival of a trigger signal from a fast photodiode (FPD) at the data acquisition equipment. The data acquisition system and a stepper motor governing the angle of the monochromator diffraction grating are both controlled by a LabView program (National Instruments).

The Raman emission from the sample is collected at an angle of approximately  $170^\circ$  from the incident laser propagation direction. In an optically thick sample, such a backscatter geometry is preferred since the emission comes primarily from target molecules near the “surface” of the sample, where there is a greatly reduced chance of reabsorption. The coaxial gas flow provides a rather sharp boundary region  $\sim 1$  mm thick between the sample and purge gas flows.

Nitrosyl chloride is easily synthesized by placing an approximately stoichiometric mixture of chlorine and NO in a reaction vessel in a dry ice–acetone bath.<sup>20</sup> Liquid CINO condenses on the vessel walls in a few minutes. When the pressure drops significantly below one atmosphere, more  $\text{Cl}_2$  and NO are added until the desired amount is obtained, typically about 50 mL of liquid CINO for our experiments. The total pressure is kept low to maintain safety. CINO is purified by slow warming while some of the vapor phase is pumped off. The remaining CINO is distilled into a new vessel, leaving insignificant amounts of less volatile components. CINO has a boiling point ( $-5.5^\circ\text{C}$ ) which is much above that of either  $\text{Cl}_2$  ( $-35^\circ\text{C}$ ) or NO ( $-101^\circ\text{C}$ ). Both reactants are therefore easily removed. The resulting CINO has a narrow melting range, indicating the absence of impurities, and no significant unidentifiable interferences occur in the Raman spectra. Temperatures are always kept sufficiently high to avoid condensation of NO, as violent reactions can occur in the liquid state.

Nitrosyl chloride is extremely corrosive, as are the reactant gases used to produce it, especially in the presence of water. Materials used in production and storage of CINO must be kept free from moisture and should be resistant to attack by acid and chlorine. Our gas regulators are made from special corrosion-resistant alloys. Other materials used in various components of the apparatus (glass, viton 3/6, stainless steel, Teflon) are all resistant to short-term chemical attack.<sup>21</sup> The primary manifold and reaction vessels are glass. Teflon stopcocks with viton O-ring seals control the gas flow in the vessels. The main gas lines supplying reactants from their storage tanks are made of stainless steel, with a few brass components. Brass O-ring adapters of our design are used with Cajon Ultra-torr seals to connect the delivery lines with the reaction vessel manifold. The CINO-saturated helium vapor flows through Teflon tubing from the storage vessel to the sample cell and from the cell to the exhaust hood. Prior to production, all gas lines and reaction

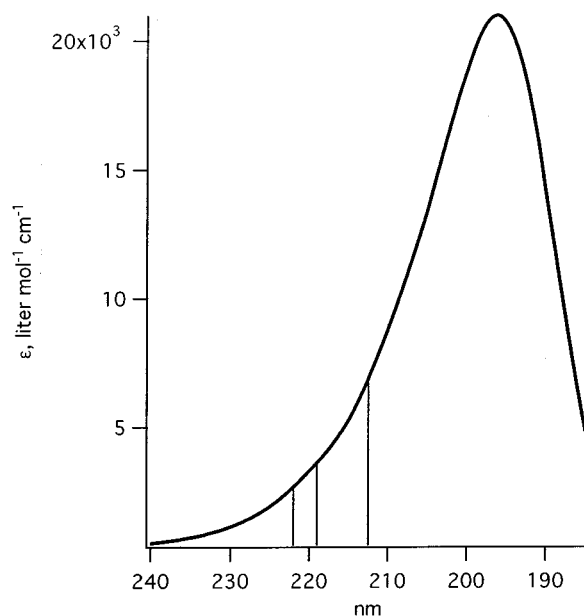


FIG. 1. The absorbance of the CINO A band, measured by Ballash *et al.* (Ref. 2). The three vertical lines at 212.5, 219, and 222 nm indicate the wavelengths used in this study.

vessels are thoroughly cleaned and oven dried. All materials are then pumped out by a diffusion pump while being heated well above 100 °C to drive away adsorbed water.

### III. CINO RAMAN SPECTRA

#### A. Results

The absorption spectrum of CINO from 15 000  $\text{cm}^{-1}$  to 53 000  $\text{cm}^{-1}$  was measured by Goodeve and Katz.<sup>1</sup> The A band was later remeasured by Ballash *et al.*, and by Tyndall *et al.*<sup>2,3</sup> Figure 1 shows the spectrum of Ballash *et al.*, with vertical lines indicating the three wavelengths of our measurements (212.5, 219, and 222 nm). These excitation wavelengths were chosen for (1) experimental accessibility, (2) resonant enhancement in the A band, and (3) avoidance of absorption bands of free NO (see Okabe<sup>22</sup>) that might be present in the cell. Raman shifts were measured out to  $\sim 3000 \text{ cm}^{-1}$ .

The Raman spectra for the three excitation wavelengths are given in Fig. 2. The spectra are vertically scaled to give the same difference in height between the maximum at 332  $\text{cm}^{-1}$  and the minimum at  $\sim 500 \text{ cm}^{-1}$ . The three spectra are qualitatively similar, especially for the first 1000  $\text{cm}^{-1}$  of Raman shift. Each spectrum was collected several times to ensure reproducibility. The centers of the Raman features for the 212 nm excitation are given in Table I with the corresponding IR absorption results and previous nonresonant Raman data.<sup>23–26</sup> The spectrum with excitation at 212 nm was chosen for comparison since it is the least congested. This study adds 12 previously unobserved bands to the 16 known bands for CINO (not including a difference band reported by Jones *et al.*,<sup>30</sup> in 1968).

Since our spectrometer could not resolve individual rotational lines, the relationship between the center of a spec-

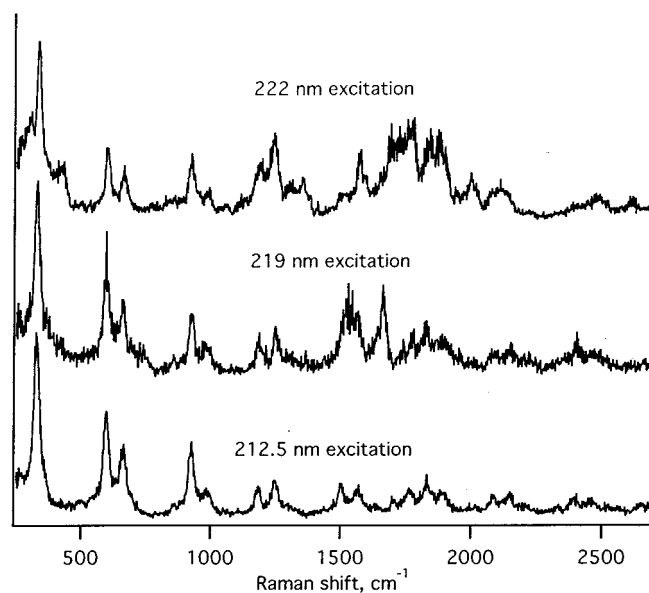


FIG. 2. Resonance Raman spectra of CINO.

tral feature and the band origin must be determined by performing a rotational band contour analysis, for which the individual rotational lines are convolved with the spectral transfer function of the monochromator.<sup>37</sup> Inertial constants for selected vibrational states of CINO are available from a variety of sources.<sup>34,38–44</sup> The asymmetry parameter for

TABLE I. Raman shifts from this study compared to bands from previous IR absorption and IR Raman data (Refs. 23–36).

Level	Vibrational frequencies ( $\text{cm}^{-1}$ )	
	This study	Previous
$\nu_3$	329.5	332.0
$\nu_2$	597.6	595.9
$2\nu_3$	661.9	
$\nu_2 + \nu_3$	926.3	
$3\nu_3$	983.5	
$2\nu_2$	1184.2	1186.5
$\nu_2 + 2\nu_3$	1249.1	
$2\nu_2 + \nu_3$	1506.0	
$\nu_2 + 3\nu_3$	1569.0	
$5\nu_3$	1640.4	
$3\nu_2$	1767.6	
$\nu_1$		1799.7
$2\nu_2 + 2\nu_3$	1833.9	1831.2
$\nu_2 + 4\nu_3$	1892.8	1894.5
$3\nu_2 + \nu_3$	2089.1	
$\nu_1 + \nu_3$		2131.1
$2\nu_2 + 3\nu_3$	2150.9	
$\nu_1 + \nu_2$	2396.7	2395.6
$\nu_1 + 2\nu_3$	2458.7	
$\nu_1 + \nu_2 + \nu_3/3\nu_2 + 3\nu_3$	2723.5	
$2\nu_1$		3563.8
$2\nu_1 + \nu_3$		3894.6
$2\nu_1 + \nu_2$		4159.7
$2\nu_1 + 2\nu_2$		4752.0
$3\nu_1$		5292.9
$3\nu_1 + \nu_3$		5623.0
$3\nu_1 + \nu_2$		5888.6
$4\nu_1$		6985.2

CINO in its ground vibrational level is  $\kappa = -0.9912$ , i.e., very close to that of a prolate symmetric top. We calculated band contours with symmetric rotor energy levels and relative oscillator strengths, assuming *a*-axis type rotational transitions. The *ab initio* results of Bai *et al.* place the transition moment near the inertial *a* axis<sup>8</sup> for the  $S_5(4^1A') \leftarrow S_0(1^1A')$  transition. The calculated band contours are insensitive to the inertial asymmetry and to small *b*-axis components of the transition moment. The Raman spectrum of methane was used to obtain an experimental instrument function for purposes of the convolution. The line shape obtained for the methane fundamental (all *Q* branch) is completely dominated by instrumental broadening and serves quite well as the spectral transfer function for use with CINO. The CINO rotational contours thus produced are in good agreement with the spectra actually measured. For all the vibrational levels we simulated, the band centers corresponded to band origins to well within the limits of experimental error. The same is expected to hold for all of the vibrational states measured in these experiments.

## B. Relation to previous studies

It has been known since flash photolysis experiments in the early 1960's that photodissociation of CINO at short wavelengths produces vibrationally excited NO.<sup>45</sup> The details of energy partitioning between product rotation, vibration, translation, and electronic energy appear to vary a great deal with wavelength across the band. A good overview of what has been done with respect to photofragment studies can be found in the paper of Skorokhodov *et al.*<sup>6</sup> and references given therein.

At 193 nm, near the center of the band, the most definitive and unambiguous results are the photofragment translational spectroscopy (PTS) results of Haas, Felder, and Huber.<sup>14</sup> They found a bimodal distribution in the product translational energy  $E_T$  and were able to fit their data to two separate components with differing values of the asymmetry parameter  $\beta$  for the angular distribution of photoproducts. A component with  $\beta \approx 0.95$  and  $\langle E_T \rangle \approx 37.4 \text{ kcal mol}^{-1}$  accounted for about 17% of the products. A second component with  $\beta \approx 0.45$  and  $\langle E_T \rangle \approx 43.1 \text{ kcal mol}^{-1}$  made up the remaining  $\sim 83\%$ . The overall  $\langle E_T \rangle$  was about  $42.1 \text{ kcal mol}^{-1}$ . The measured  $E_T$  distribution was decomposed into individual vibrational components by assuming that the molecules had a distribution of rotational energies with an average rotational energy  $E_R \sim 5 \text{ kcal mol}^{-1}$  and FWHM of  $\sim 4.6 \text{ kcal mol}^{-1}$ , irrespective of vibrational state. The result is an estimate of about  $63.6 \text{ kcal mol}^{-1}$  for  $\langle E_V \rangle$ . This is a significantly higher value than would be derived from the results of Gillan *et al.*,<sup>11</sup> who used laser induced fluorescence on rotationally and translationally relaxed NO products to determine  $\langle E_V \rangle$ . Their vibrational distribution is, in turn, skewed towards higher *v* than the distribution given by Moser *et al.*,<sup>10</sup> who measured infrared emission from rotationally relaxed products. Gillan *et al.* persuasively show, however, that at least the lowest *v* states observed by Moser *et al.*, were produced by secondary processes and were not present in the nascent distribution. Thus, the details of the energy distribution amongst the product's degrees of freedom is still some-

what in question, even near band center. The existence of two channels with different values of  $\beta$  and different distributions of  $E_T$  seems to be unambiguous. Haas *et al.* say this can arise either from initial excitation into two different electronic states or from initial excitation to a single excited electronic state followed by nonadiabatic leakage of part of the amplitude onto a second PES. They favor the first of these possibilities and speculate that one channel may produce ground-state  $\text{Cl}(^2P_{3/2})$  and the other excited  $\text{Cl}(^2P_{1/2})$ .

To a first approximation, the angular distribution of products is a snapshot of the initial distribution of orientations of the transition moment in spaced-fixed coordinates (averaged over the ensemble of rotational states). Hence, the idea that excitation at band center involves two excited electronic states in proportions of about 1:5 seems fairly compelling. It is, however, at odds with the *ab initio* calculations of Bai *et al.* on the CINO molecule.<sup>7,8</sup> While Bai's results indicate three excited electronic states with roughly the correct energy, the relative intensities are calculated to be in the ratio  $1:10^{-3}:0$  (the last value because the excited state is a triplet). Despite any shortcomings of the basis sets used and the absence of spin-orbit terms in the *ab initio* calculation, it is difficult to see how the results could be off by such a large factor in the relative intensities. An alternative explanation, whose plausibility is difficult to assess, is initial excitation to a single PES with subsequent evolution into two separate components with different average rotational periods during photodissociation, either remaining on the same PES or with one of the components representing nonadiabatic transfer to another electronic state.

Felder and Morley<sup>5</sup> used the same apparatus as Haas, Felder, and Huber for PTS at 248 nm. At this wavelength, the absorption cross section is only about  $3.8 \times 10^{-19} \text{ cm}^2$ , which raises a question whether it should be considered part of the same band at all. They found a bimodal  $E_T$  distribution (actually a single peak with a long tail to low  $E_T$ ), with the minor component having a relative importance of 20%. The asymmetry parameter  $\beta$  for the major component was  $\sim 1.2$ . The  $\beta$  value for the minor component was less well determined, but appeared to be about the same. Felder and Morley proposed a total of three excited electronic states to account for the entire A band. They called these  $A_a$ ,  $A_b$ , and  $A_c$  in increasing order of energy, and attributed  $A_c$  to the Bai *et al.* strong  $S_5(4^1A') \leftarrow S_0(1^1A')$  transition.  $A_b$  and  $A_a$  were assigned as  $S_4(3^1A') \leftarrow S_0(1^1A')$  and  $T_5(3^3A') \leftarrow S_0(1^1A')$ , respectively.

These authors proposed that the absorption at 193 nm owes 83% to  $A_c$  and  $\sim 17\%$  to  $A_b$ . At 248 nm, they assign 80% to  $A_a$  and 20% to  $A_b$ . Noting that the average internal (rovibrational) energy of the NO is a much larger fraction of the total energy at 193 nm than at 248 nm, they predicted that<sup>5</sup> "the Raman spectrum at 248 nm, in contrast to the one obtained at 266 nm, should begin to show a weak progression in the  $\nu_1$  mode, which should become even more important at shorter wavelengths." This prediction is not borne out by the present investigation. The  $\nu_1$  mode is seen only in combination bands with the other modes.

Skorokhodov *et al.*<sup>6</sup> performed two kinds of measurements that allowed specific detection of  $\text{Cl}(^2P_{3/2})$  and

Cl\*( $^2P_{1/2}$ ): (1) Photofragment imaging<sup>46</sup> using REMPI detection, and (2) VUV-LIF determination of the Cl\*/Cl ratio. The results indicated a Cl\*/Cl ratio of  $\sim 0.9$  for dissociation at 212.56 nm, of  $\sim 0.45$  at 235 nm and of  $\sim 1.1$  at 248 nm. For photodissociation at  $\sim 235$  nm, both Cl and Cl\* have bimodal distributions of  $E_T$ . The low  $E_T$  component for Cl\* had  $\beta \approx 1.8$  and the high  $E_T$  component had  $\beta \approx 1.5$ . The angular distribution for Cl was similar, leading to the interpretation that all four components arise from a single electronic transition, i.e., the state called  $A_b$  by Felder and Morley. The signal for dissociation at  $\sim 211$  nm was too poor to obtain a definite value of  $\beta$ , though it was reported to be low. This similarity to the situation at 193 nm led Skorokhodov *et al.*, to assign all the action at both 193 nm and 211 nm to the single dominant surface  $A_c$ . They attribute the dissociation at 235 nm to  $A_b$ , and that at 248 nm to  $A_a$  and  $A_b$ .

The lack of any significant electronic interference in the Raman fundamentals measured here suggests that only one state is dominant (although possibly multiple states characterized by nearly parallel PES's) in the region 212–222 nm. This abuts the wavelength region assigned by Skorokhodov *et al.*, and so would be  $A_c$  under their assignment. This then requires that the crossover to dominance of the  $A_b$  transitions must occur in the narrow wavelength range 222–235 nm. Further analysis of the electronic state implications must await quantitative modeling that is beyond the scope of the present paper.

## IV. VIBRATIONAL ANALYSIS

### A. Background

Bailey and Cassie measured the first IR absorption spectrum of CINO in 1934.<sup>47</sup> Since that time, upwards of 20 individual studies have dealt with various aspects of the vibrational and rotational absorption spectrum. A comprehensive overview of work up to 1986 is given by McDonald *et al.*,<sup>33</sup> although a number of further studies have occurred since this paper was published.

Jones *et al.*, published the first Dunham expansion for the vibrational terms of CINO in 1968, giving harmonic frequencies and first order anharmonicity constants.<sup>30</sup> Their fit used 17 transitions for  $^{16}\text{O}^{14}\text{N}^{35}\text{Cl}$  (all that were known at the time), including the  $\nu_1 - \nu_2$  difference band. We have combined our Raman data with earlier data to produce a revised Dunham expansion:

$$G(v_1, v_2, v_3) = \sum_{k=1}^3 \omega_k (v_k + 1/2) + \sum_k \sum_{j \geq k}^3 x_{kj} (v_k + 1/2) \times (v_j + 1/2). \quad (1)$$

Table II gives the Dunham coefficients found by Jones *et al.*, our Dunham coefficients obtained from the larger set of levels, and the standard deviations for the parameters in our fit. There are nine independently adjustable parameters to fit 28 spectral features. All  $\omega$  values are well determined, as are  $x_{11}$ ,  $x_{22}$ , and  $x_{23}$ . The values of  $x_{12}$ ,  $x_{13}$ , and  $x_{33}$  are poorly determined. The value of  $x_{13}$  is not significantly different from zero.

TABLE II. Dunham coefficients for CINO: Jones *et al.* (Ref. 30) this study, and standard deviations for this study. All values are in  $\text{cm}^{-1}$ .

Coefficient	Jones <i>et al.</i>	This work	Std. dev.
$\omega_1$	1835.6	1831.6	3.8
$\omega_2$	603.2	600.4	3.9
$\omega_3$	336.4	331.2	2.9
$x_{11}$	-17.8	-17.4	0.5
$x_{12}$	0.0	1.2	0.9
$x_{13}$	-0.6	0.7	1.0
$x_{22}$	-2.6	-2.7	0.7
$x_{23}$	-4.3	-3.1	0.7
$x_{33}$	-1.0	-0.5	0.3

The results of our fit are compared with the observed peak positions in Table III. The largest magnitude of deviation is  $4.1 \text{ cm}^{-1}$ . For features that were present both in our data and the previous data, the more precise IR data were used in the fitting procedure.

The ability of this simple Dunham expansion to fit the levels might be taken as an indication that CINO could adequately be described in terms of normal coordinates. We know, however, that the highest energy levels observed must correspond to large amplitude excursions from the equilibrium geometry—a situation that is seldom if ever well described by normal coordinates. What is more, even in the lower-energy ground state vibrations, normal coordinate analyses have produced controversy about the assignment of the modes. McDonald *et al.*, have recently and definitively assigned  $\nu_3$  ( $330 \text{ cm}^{-1}$ ) as a Cl–N stretching mode and  $\nu_2$  ( $600 \text{ cm}^{-1}$ ) as a “scissoring” motion pivoting on nitrogen,

TABLE III. Spectral features, the predicted locations from our Dunham expansion, and differences. All values are in  $\text{cm}^{-1}$ .

Level	Observed	Calculated	Difference
$\nu_3$	332.0	332.6	0.6
$\nu_2$	595.9	598.3	2.4
$2\nu_3$	661.9	659.2	-2.7
$\nu_2 + \nu_3$	926.3	922.6	-3.7
$3\nu_3$	983.5	985.9	2.4
$2\nu_2$	1186.5	1186.0	-0.5
$\nu_2 + 2\nu_3$	1249.1	1246.9	-2.2
$2\nu_2 + \nu_3$	1506.0	1507.9	1.9
$\nu_2 + 3\nu_3$	1569.0	1571.1	2.1
$5\nu_3$	1640.4	1639.1	-1.3
$3\nu_2$	1767.6	1769.0	1.4
$\nu_1$	1799.7	1801.8	2.1
$2\nu_2 + 2\nu_3$	1833.9	1829.8	-4.1
$\nu_2 + 4\nu_3$	1892.8	1895.4	2.6
$3\nu_2 + \nu_3$	2089.1	2088.6	-0.5
$\nu_1 + \nu_3$	2131.1	2130.3	-0.8
$2\nu_2 + 3\nu_3$	2150.9	2151.8	0.9
$\nu_1 + \nu_2$	2395.6	2396.0	0.5
$\nu_1 + 2\nu_3$	2458.7	2458.7	0.0
$2\nu_1$	3563.8	3563.7	-0.1
$2\nu_1 + \nu_3$	3894.6	3894.0	-0.6
$2\nu_1 + \nu_2$	4159.7	4159.8	0.1
$2\nu_1 + 2\nu_2$	4752.0	4751.2	-0.8
$3\nu_1$	5292.9	5291.5	-1.4
$3\nu_1 + \nu_3$	5623.0	5623.6	0.6
$3\nu_1 + \nu_2$	5888.6	5889.5	0.9
$4\nu_1$	6985.2	6985.4	0.2

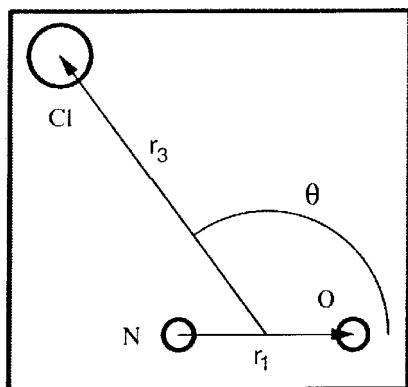


FIG. 3. The ClNO Jacobi coordinates.

but they point out that this leads to an unusually low stretching frequency and an unusually high bending frequency for a molecule with constituent atoms of these masses.<sup>33</sup> It is rare but not unknown for a bending mode to have a higher frequency than a stretching mode. Our Raman spectra with A band excitation reflect dynamics in the excited state(s) following absorption of a photon. These spectra show more overtone and combination activity in  $\nu_3$  than in  $\nu_2$ , thus supporting the assignment of this mode as largely a Cl–N stretching motion.

In their exploration of the stretch vs bend issue, McDonald *et al.*, performed a number of calculations.<sup>33</sup> First, they attempted a normal mode fit assigning the  $\nu_3$  mode as the bend and the  $\nu_2$  mode as the N–Cl stretch. The result failed to reproduce the observed rotational distortion constants. Another attempt, using the bend for  $\nu_2$  and the N–Cl stretch for  $\nu_3$  produced satisfactory results with four adjustable parameters, including an interaction term coupling the N–Cl stretch and the bend. Finally, a third force field was generated, using the three bond lengths (N–Cl, N–O, and Cl–O) as (nonorthogonal) coordinates. A potential energy distribution analysis for this model indicated that the  $\nu_2$  normal mode was a strong mixture of the N–Cl and N–O stretches. In their words “It is clear that the choice of a model and the interpretation of the physical significance of a model must be done carefully especially for a molecule like ONCI.”

## B. Jacobi coordinates

We have chosen to describe the system in Jacobi coordinates. This choice is natural for describing the atom–diatomic molecule products as the system proceeds towards dissociation but also turns out to provide an adequate description in the neighborhood of the ground-state equilibrium geometry. Jacobi coordinates explicitly include the ability to describe large amplitude motions.<sup>48</sup> In the specific case of ClNO, the two Jacobi vectors are  $\vec{r}_1$ , which points from N to O, and  $\vec{r}_3$  which points from the NO center of mass to Cl (see Fig. 3). In a purely impulsive model of the dissociation taken strictly along the  $\vec{r}_3$  direction, there is no torque on the NO fragment upon dissociation since the impulse is “against” the NO center of mass. (This does not mean, however, that the NO fragment will have no rotational motion,

since the angular momentum of the parent molecule must be conserved.) Jacobi coordinates have been used to describe the dissociation in other bands of ClNO which show little rotational excitation beyond the initial thermal distribution.<sup>49–51</sup>

The lengths  $r_1$  and  $r_3$  and the angle  $\theta$  between  $\vec{r}_1$  and  $\vec{r}_3$  provide three (curvilinear but orthogonal) vibrational coordinates for describing the vibrational modes. (The subscripts on the Jacobi coordinates are chosen so that  $r_1$  correlates to the  $\nu_1$  vibrational mode and  $r_3$  to  $\nu_3$ .) In general, all three Jacobi coordinates will be coupled in the molecular region of the potential surface, though there are some indications that  $r_1$  is only weakly coupled to the other two coordinates: the NO bond is found to have similar lengths in the diatomic (1.1508 Å, Herzberg<sup>52</sup>) and triatomic (1.1405 Å, Jones<sup>30</sup>) molecules; the  $\nu_1$  mode is found to be a very minor player in the resonance Raman spectra, indicating that there is not a great deal of change of the NO bond length during the early femtoseconds of the excited state dynamics.

For  $z = \cos(\theta)$  and for volume element  $dr_1 dr_2 dz$ , the vibrational kinetic energy in Jacobi coordinates is

$$T = -\frac{\hbar^2}{2\mu_1} \frac{\partial^2}{\partial r_1^2} - \frac{\hbar^2}{2\mu_3} \frac{\partial^2}{\partial r_3^2} - \frac{\hbar^2}{2} \left( \frac{1}{\mu_1 r_1^2} + \frac{1}{\mu_3 r_3^2} \right) \frac{\partial}{\partial z} (1-z^2) \frac{\partial}{\partial z}, \quad (2)$$

where  $\mu_1$  is the reduced mass of NO and  $\mu_3$  is the reduced mass of Cl and NO. Kinetic coupling between the coordinates occurs only from the  $r_1^{-2}$  and  $r_3^{-2}$  terms in the bending kinetic energy. Replacing these by  $r_{1e}^{-2}$  and  $r_{3e}^{-2}$ , respectively, allows an approximately separable model for describing the vibrational levels.

For a crude first approximation employing this separable kinetic energy expression, we used the potential

$$V' = c_{200} [1 - \exp(-a_1(r_1 - r_{1e}))]^2 + c_{020}(r_3 - r_{3e})^2 + c_{002}(z - z_e)^2, \quad (3)$$

where  $r_{1e} = 1.1405$  Å,  $r_{3e} = 2.2828$  Å, and  $z_e = -0.60749$ . The remaining parameters were adjusted to optimize a fit to the known bands. Since the anharmonicity of  $\nu_1$  is well-determined from the Dunham expansion, the  $r_1$  mode was modelled as a Morse oscillator. This procedure yielded a physically reasonable starting point in the iterative optimization of parameters for the more general potential of the form

$$V = \sum_i \sum_j \sum_k c_{ijk} [1 - \exp(-a_1(r_1 - r_{1e}))]^i \times (r_3 - r_{3e})^j (z - z_e)^k \quad (4)$$

suitable for modelling all observed bands including combination bands. The kinetic coupling in Eq. (2) was also fully included at the same time. Vibrational eigenvalues for this potential were then determined using a large-amplitude vibrational basis.

We followed the strategy of Johnson and Reinhardt<sup>53,54</sup> in using Laguerre bases of exponential arguments for radial coordinates and Jacobi polynomial bases for the angular coordinate. Basis set parameters and number of configurations

TABLE IV. Nonzero potential parameters for the fit in Jacobi coordinates.

$a_1$	$2.7924 \text{ \AA}^{-1}$	$c_{200}$	$47\,874 \text{ cm}^{-1}$
$c_{020}$	$26\,325 \text{ cm}^{-1} \text{ \AA}^{-2}$	$c_{030}$	$-336.3 \text{ cm}^{-1} \text{ \AA}^{-3}$
$c_{002}$	$74\,555 \text{ cm}^{-1}$	$c_{004}$	$0.7083 \text{ cm}^{-1}$
$c_{202}$	$4750 \text{ cm}^{-1}$	$c_{022}$	$170.8 \text{ cm}^{-1} \text{ \AA}^{-2}$

(products of primitive basis functions in the three individual vibrational coordinates) were optimized in bootstrap fashion to ensure convergence to within  $\sim 0.1 \text{ cm}^{-1}$  of the eigenvalues corresponding to all observed vibrational transitions. A total of 898 basis functions were ultimately used. For a fixed set of parameters describing the basis functions and a fixed basis size, the potential parameters were varied. The optimization was occasionally interrupted to verify that all of the relevant eigenvalues were well converged. The potential optimization, as judged by mean square error of the calculated transitions, first emphasized the fundamentals. Then overtones were added, and finally the combination bands. Several higher order and cross terms in the potential were tested individually and in combination to see whether they significantly improved the fit.

The best fit balancing the competing goals of minimum error and minimum number of parameters was achieved with a potential that had eight adjustable parameters. The best fit values of these parameters are given in Table IV. Table V compares the fit to experimental data. The rms deviation for the whole set of vibrational terms is  $2.71 \text{ cm}^{-1}$ . The largest deviation from a spectral feature is an underestimate by

TABLE V. Observed spectral features, calculated values from fit, and differences, in units of  $\text{cm}^{-1}$ .

Level	Observed	Calculated	Difference
$\nu_3$	332.0	329.5	-2.5
$\nu_2$	595.9	595.6	-0.3
$2\nu_3$	661.9	658.0	-3.8
$\nu_2 + \nu_3$	926.3	922.4	-3.9
$3\nu_3$	983.5	985.8	2.3
$2\nu_2$	1186.5	1185.1	-1.4
$\nu_2 + 2\nu_3$	1249.1	1248.4	-0.7
$2\nu_2 + \nu_3$	1506.0	1509.4	3.4
$\nu_2 + 3\nu_3$	1569.0	1573.5	4.5
$5\nu_3$	1640.4	1638.5	-1.9
$3\nu_2$	1767.6	1768.5	0.9
$\nu_1$	1799.7	1800.2	0.5
$2\nu_2 + 2\nu_3$	1833.9	1832.7	-1.2
$\nu_2 + 4\nu_3$	1892.8	1897.6	4.8
$3\nu_2 + \nu_3$	2089.1	2090.2	1.1
$\nu_1 + \nu_3$	2131.1	2129.7	-1.4
$2\nu_2 + 3\nu_3$	2150.9	2155.1	4.2
$\nu_1 + \nu_2$	2395.6	2394.5	-1.1
$\nu_1 + 2\nu_3$	2458.7	2458.3	-0.4
$2\nu_1$	3563.8	3567.9	4.1
$2\nu_1 + \nu_3$	3894.6	3895.3	0.8
$2\nu_1 + \nu_2$	4159.7	4159.4	-0.3
$2\nu_1 + 2\nu_2$	4752.0	4749.0	-3.0
$3\nu_1$	5292.9	5295.4	2.5
$3\nu_1 + \nu_3$	5623.0	5624.0	1.0
$3\nu_1 + \nu_2$	5888.6	5883.6	-5.0
$4\nu_1$	6985.2	6989.0	3.8

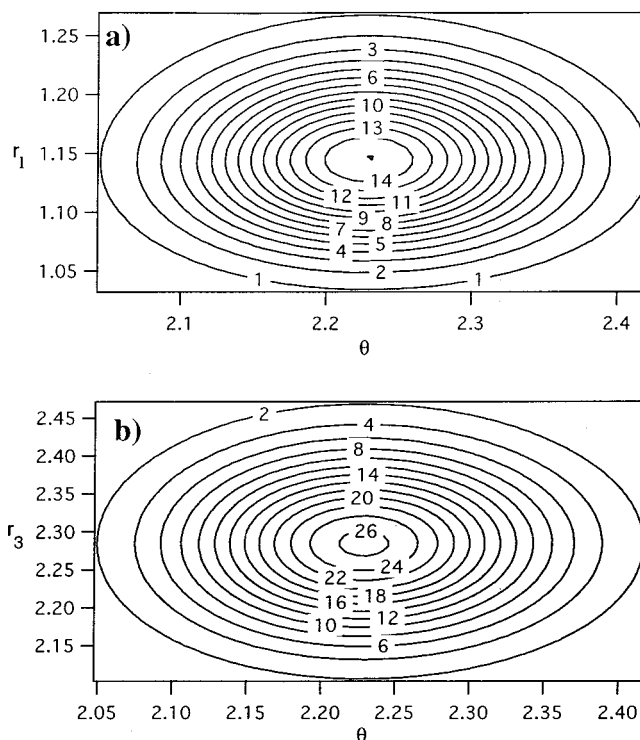


FIG. 4. The ground state wave function contours. (a)  $r_1$  vs  $\theta$  with  $r_3$  fixed at  $2.2 \text{ \AA}$ . (b)  $r_3$  vs  $\theta$  with  $r_1$  fixed at  $1.14 \text{ \AA}$ .  $\theta$  is in radians,  $r_1$  and  $r_3$  are in  $\text{\AA}$ .

about  $5 \text{ cm}^{-1}$  for the  $3\nu_1 + \nu_2$  combination band. Contour plots of the ground state and selected excited state wave functions are shown in Figs. 4–6.

A small-amplitude expansion of our potential allows a normal modes calculation that can be compared directly to that of other investigators. Figure 7 compares our stick diagrams obtained in this way with those arrived at by McDonald *et al.*<sup>31</sup> The two sets of normal coordinates are quite similar. The two  $\nu_1$  normal coordinates are virtually identical, as they should be since both coordinate systems take  $q_1$  as the pure N–O stretch. Perhaps the most prominent difference in the diagrams is the  $\nu_3$  mode. Our assignment for the  $\nu_3$  fit is obviously the Jacobi stretch, involving no change in the N–O distance. The results of Jones *et al.* for  $\nu_3$  is a mode that appears to have some slight bending character, with nitrogen relatively stationary while chlorine and oxygen move generally away (and toward) each other.

Because of the relatively weak coupling between the Jacobi coordinates in the numerically converged large-amplitude vibrational calculations, the Jacobi coordinates are identified as “good” coordinates for the ground electronic state of nitrosyl chloride. The potential in these coordinates is physically reasonable, has relatively small coupling constants, and sufficiently describes all measured vibrational spectra to good accuracy. Moreover, the modal structure of the vibrational wave functions (Figs. 4–6) clearly aligns along the appropriate coordinate axes with no significant distortion. This is salutary because Jacobi coordinates are the natural choice for describing the photodissociation process in the A band.

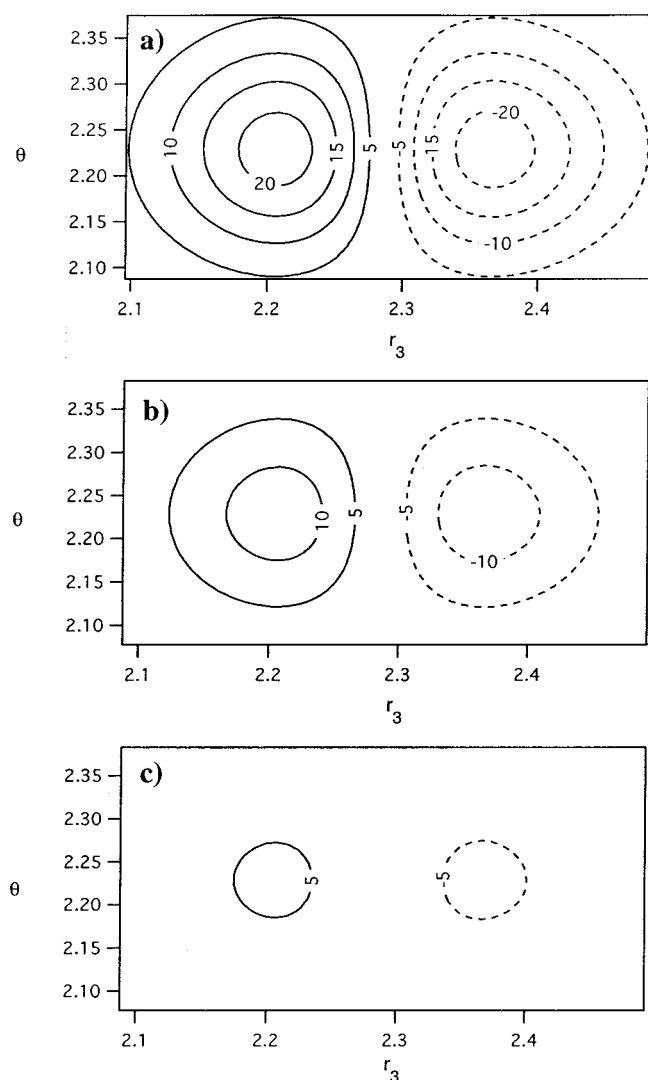


FIG. 5. The first excited state, corresponding to excitation of the  $\nu_3$  mode, showing  $\theta$  vs  $r_3$ .  $\theta$  is in radians,  $r_3$  in Å. (a)  $r_1 = 1.14$  Å, (b)  $r_1 = 1.2$  Å, (c)  $r_1 = 1.23$  Å.

## V. DISCUSSION

Resonance Raman spectra have been obtained for CINO at three wavelengths in the ultraviolet A band. Twelve previously unobserved vibrational levels in the ground state have been observed. These new levels, together with previously known vibrational levels, allowed the construction of a large amplitude vibrational model valid in and beyond the Franck–Condon region. The ground state surface shows a large degree of separability in Jacobi coordinates even in the triatomic molecular region; this finding bears directly upon previous difficulties in identifying the  $\nu_2$  and  $\nu_3$  modes. This ground-state PES and its vibrational eigenvalues will become the foundation of an effort to model the photodissociation dynamics in the upper electronic state(s).

Although the work reported here concentrates primarily on the vibrational levels of the electronic ground state, there are a couple of clues to the dynamic behavior of electronically excited CINO in the pattern of levels observed and their relative intensities. The absence of any observable activity in the  $\nu_1$  fundamental is somewhat surprising in view

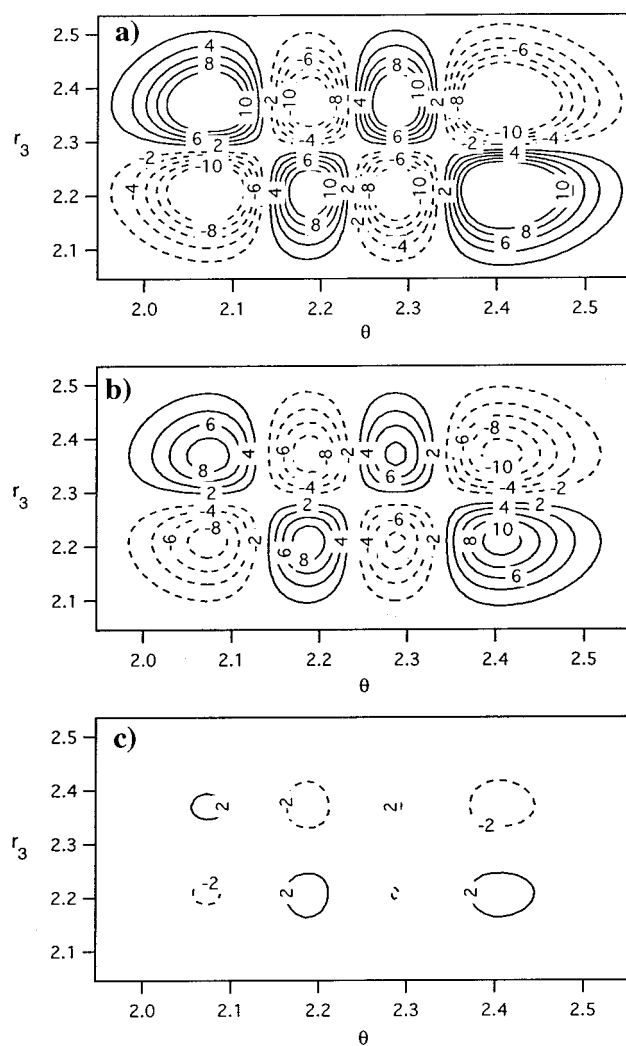


FIG. 6. The 17th excited state, corresponding to one quantum of excitation in the  $\nu_3$  mode and three quanta in the  $\nu_2$  mode. Shown is  $r_3$  vs  $\theta$ .  $\theta$  is in radians,  $r_3$  in Å. (a)  $r_1 = 1.14$  Å, (b)  $r_1 = 1.2$  Å, (c)  $r_1 = 1.25$  Å. This corresponds to the 15th entry in Table V.

of the strong evidence of vibrational excitation in the NO photoproduct. The  $\nu_1$  mode does show up in overtones and combination bands. This is reminiscent of the behavior of the  $\nu_2$  umbrella bending mode in  $\text{CH}_3\text{I}$ ,<sup>55</sup> i.e., absence of the fundamental, but appearance of the mode in combination with the C–I stretch. This was taken to indicate that motion in the umbrella angle did not occur immediately upon excitation, but started to develop only when the C–I bond angle had lengthened from its ground-state equilibrium value. The same reasoning would apply for CINO. The behavior of the  $\nu_1$  mode seems to indicate that motion in the  $r_1$  coordinate is not occurring in the first few fs of evolution, but develops later in the course of the photodissociation.

The Raman spectra may also have some bearing on the question of whether more than one electronically excited state is operative near the center of the A band. Simultaneous excitation of more than one excited electronic state sets up the possibility of interference between amplitudes evolving in the two different states. This has clearly been seen in the case of  $\text{CH}_3\text{I}$  (Ref. 14) and higher alkyl iodides.<sup>13</sup> No such

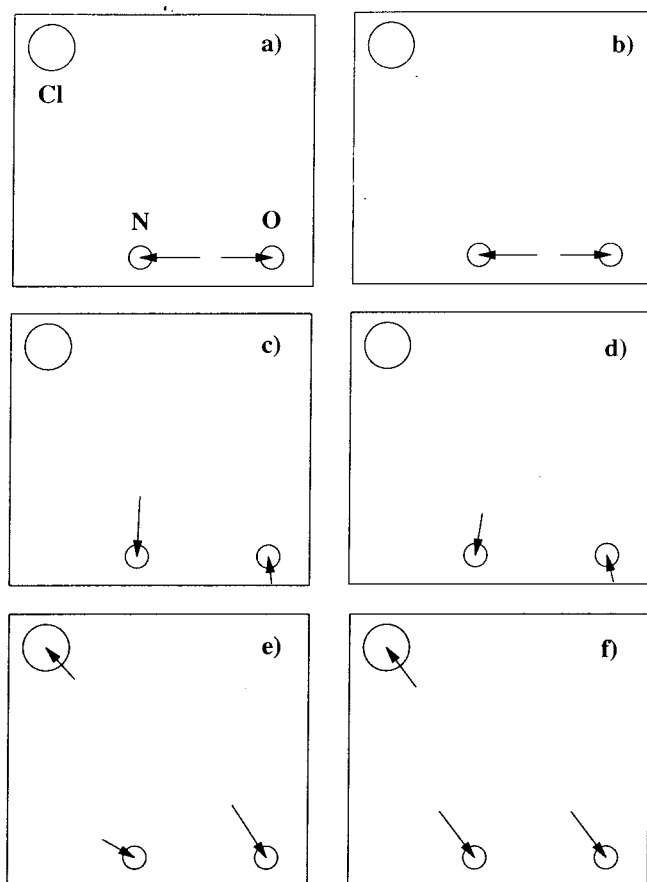


FIG. 7. Comparing the normal modes of McDonald *et al.*, with the Jacobi coordinates found in this study. (a) and (b) are the N–O stretches in each coordinate system and are virtually identical. (c) is McDonald's Cl–N–O bend. (d) is the Jacobi bend. (e) is McDonald's N–Cl stretch, while (f) is the Jacobi Cl–(NO) stretch. In (a) through (d) the chlorine atom appears to be stationary because to make its motion visible would make the other motion arrows extend beyond the figure's border.

interference effects are evident in the ClNO results. While absence of interferences does not conclusively rule out participation of more than one excited electronic state in the absorption, it weighs in on that side of the issue, at least insofar as the absorption and early dynamical evolution is concerned. On the basis of this evidence, therefore, we prefer a picture in which the initial excitation for these wavelengths is predominantly to a single excited electronic state, Bai's  $S_5(4^1A')$ . In order to account for the observed bimodal distribution in  $E_T$  and the different  $\beta$  parameters for the two components, one would then have to postulate either bifurcation of the evolving wave packet into two pieces on that surface or nonadiabatic transfer of part of the amplitude to another electronic PES. In either case, the difference in  $\beta$  parameters could only be understood if the two channels involved significant differences in the amount of molecular rotation (of the triatomic entity) during the course of the dissociation.

We are in the process of constructing a code for time-dependent propagation in curvilinear coordinates using wavelets.<sup>56</sup> This will be used to model the observed Raman spectra, determining the minimum number of PES's required. Solution of the time-dependent Schrödinger equation

and Fourier transformation to obtain Raman scattering amplitudes<sup>15–17,57</sup> provides for comparison with the observed patterns of intensity.

## ACKNOWLEDGMENTS

Grateful acknowledgment is made to the National Science Foundation and the Robert A. Welch Foundation for support of this work.

- <sup>1</sup>C. F. Goodeve and S. Katz, Proc. R. Soc. London, Ser. A **172**, 432 (1939).
- <sup>2</sup>N. M. Ballash and D. A. Armstrong, Spectrochim. Acta, Part A **30**, 941 (1974).
- <sup>3</sup>G. S. Tyndall, K. M. Stedman, W. Schneider, J. P. Burrows, and G. K. Moortgat, J. Photochem. **36**, 133 (1987).
- <sup>4</sup>B.-M. Haas, P. Felder, and J. R. Huber, Chem. Phys. Lett. **180**, 293 (1991).
- <sup>5</sup>P. Felder and G. P. Morley, Chem. Phys. **185**, 145 (1994).
- <sup>6</sup>V. Skorokhodov, Y. Sato, K. Suto, Y. Matsumi, and M. Kawasaki, J. Phys. Chem. **100**, 12321 (1996).
- <sup>7</sup>D. Solgadi, F. Lahmani, C. Lardeux, and J. P. Flament, Chem. Phys. **79**, 225 (1983).
- <sup>8</sup>Y. Y. Bai, A. Ogai, C. X. W. Qian, L. Iwata, G. A. Segal, and H. Reisler, J. Chem. Phys. **90**, 3903 (1989).
- <sup>9</sup>L. Werner, B. Wunderer, and H. Walther, Chem. Phys. **60**, 109 (1981).
- <sup>10</sup>M. D. Moser, E. Weitz, and G. C. Schatz, J. Chem. Phys. **78**, 757 (1983).
- <sup>11</sup>I. T. F. Gillan, D. J. Denvir, H. F. J. Cormican, I. Duncan, and T. Morrow, Chem. Phys. **167**, 193 (1992).
- <sup>12</sup>H. L. Kim, Y. Mo, Y. Matsumi, and M. Kawasaki, Bull. Korean Chem. Soc. **13**, 162 (1992).
- <sup>13</sup>D. L. Phillips and A. B. Myers, J. Chem. Phys. **95**, 226 (1991).
- <sup>14</sup>G. E. Galica, B. R. Johnson, M. O. Hale, and J. L. Kinsey, J. Phys. Chem. **95**, 7994 (1991).
- <sup>15</sup>E. J. Heller, Acc. Chem. Res. **14**, 368 (1981).
- <sup>16</sup>E. J. Heller, in *Potential Energy Surfaces and Dynamics Calculations*, edited by D. G. Truhlar (Plenum, New York, 1981).
- <sup>17</sup>E. J. Heller, R. L. Sundberg, and D. Tannor, J. Phys. Chem. **86**, 1822 (1982).
- <sup>18</sup>B. R. Johnson, C. Kittrell, P. B. Kelly, and J. L. Kinsey, J. Phys. Chem. **100**, 7743 (1996).
- <sup>19</sup>A. J. Bell and J. G. Frey, Mol. Phys. **69**, 943 (1990).
- <sup>20</sup>D. A. Baugh (private communication).
- <sup>21</sup>Houston Valve Company, Corrosion Charts, 1996.
- <sup>22</sup>H. Okabe, *Photochemistry of Small Molecules* (Wiley, New York, 1978).
- <sup>23</sup>C. M. Beeson and D. M. Yost, J. Chem. Phys. **7**, 44 (1939).
- <sup>24</sup>P. Botschwina, H. Haertner, and W. Sawodny, Chem. Phys. Lett. **74**, 156 (1980).
- <sup>25</sup>W. G. Burns and H. J. Bernstein, J. Chem. Phys. **18**, 1669 (1950).
- <sup>26</sup>J. R. Durig and R. C. Lord, Spectrochim. Acta **19**, 421 (1963).
- <sup>27</sup>W. H. Eberhardt and T. G. Burke, J. Chem. Phys. **20**, 529 (1952).
- <sup>28</sup>M. Feuerhahn, W. Hilbig, R. Minkwitz, and U. Engelhardt, Spectrochim. Acta, Part A **34**, 1065 (1978).
- <sup>29</sup>I. C. Hisatsune and P. Miller, Jr., J. Chem. Phys. **38**, 49 (1963).
- <sup>30</sup>L. H. Jones, R. R. Ryan, and L. B. Asprey, J. Chem. Phys. **49**, 581 (1968).
- <sup>31</sup>L. H. Jones and B. I. Swanson, J. Phys. Chem. **95**, 86 (1991).
- <sup>32</sup>L. Landau and W. H. Fletcher, J. Mol. Spectrosc. **4**, 276 (1960).
- <sup>33</sup>J. K. McDonald, J. A. Merritt, V. F. Kalasinsky, H. L. Heusel, and J. R. Durig, J. Mol. Spectrosc. **117**, 69 (1986).
- <sup>34</sup>A. M. Mirri and E. Mazzariol, Spectrochim. Acta **22**, 785 (1966).
- <sup>35</sup>A. G. Pulford and A. Walsh, Trans. Faraday Soc. **47**, 347 (1951).
- <sup>36</sup>J. H. Wise and J. T. Elmer, J. Chem. Phys. **18**, 1411 (1950).
- <sup>37</sup>J. E. Stewart, *Infrared Spectroscopy* (Marcel Dekker, New York, 1970).
- <sup>38</sup>G. L. Bendazzoli, G. Cazzoli, C. D. Esposti, G. Fano, F. Ortolani, and P. Palmieri, J. Chem. Phys. **84**, 5351 (1986).
- <sup>39</sup>G. Cazzoli, C. Degli Esposti, D. Dmiani, and A. M. Mirri, Chem. Phys. Lett. **80**, 365 (1981).
- <sup>40</sup>G. Cazzoli, C. Degli Esposti, P. Palmieri, and S. Simeone, J. Mol. Spectrosc. **97**, 165 (1983).
- <sup>41</sup>B. Gatehouse, H. S. P. Muller, N. Heineking, and M. C. L. Gerry, J. Chem. Soc., Faraday Trans. **91**, 3347 (1995).

- <sup>42</sup>A. M. Mirri, R. Carvellati, and G. Cazzoli, *J. Mol. Spectrosc.* **71**, 386 (1978).
- <sup>43</sup>A. M. Mirri, R. Cervellati, and G. Cazzoli, *J. Mol. Spectrosc.* **83**, 202 (1980).
- <sup>44</sup>J. D. Rogers, W. J. Pietenpol, and D. Williams, *Phys. Rev.* **83**, 431 (1951).
- <sup>45</sup>N. Basco and R. G. W. Norrish, *Proc. R. Soc. London, Ser. A* **268**, 291 (1962).
- <sup>46</sup>D. W. Chandler and P. L. Houston, *J. Chem. Phys.* **87**, 1445 (1987).
- <sup>47</sup>C. R. Bailey and A. B. D. Cassie, *Proc. R. Soc. London* **145A**, 336 (1934).
- <sup>48</sup>R. Schinke, *Photodissociation Dynamics: Spectroscopy and Fragmentation of Small Polyatomic Molecules* (Cambridge University Press, New York, 1993).
- <sup>49</sup>U. Manthe, H.-D. Meyer, and L. S. Cederbaum, *J. Chem. Phys.* **97**, 3199 (1992).
- <sup>50</sup>C. X. W. Qian, A. Ogai, L. Iwata, and H. Reisler, *J. Chem. Phys.* **92**, 4296 (1990).
- <sup>51</sup>D. Solter, H.-J. Werner, M. von Dirke, A. Untch, A. Vegiri, and R. Schinke, *J. Chem. Phys.* **97**, 3357 (1992).
- <sup>52</sup>G. Herzberg, *Molecular Spectra and Molecular Structure I. Spectra of Diatomic Molecules*, 2nd ed. (Krieger, Melbourne, 1989).
- <sup>53</sup>B. R. Johnson and W. P. Reinhardt, *J. Chem. Phys.* **85**, 4538 (1986).
- <sup>54</sup>B. R. Johnson, *J. Chem. Phys.* **92**, 574 (1990).
- <sup>55</sup>D. Imre, J. L. Kinsey, A. Sinha, and J. Krenos, *J. Phys. Chem.* **88**, 3956 (1984).
- <sup>56</sup>B. R. Johnson, J. L. Mackey, and J. L. Kinsey, *J. Comp. Phys.* (to be published).
- <sup>57</sup>E. J. Heller, *J. Chem. Phys.* **62**, 1544 (1975).